

Quantum phenomena in magnetic nano clusters

C RAGHU¹, INDRANIL RUDRA¹, DIPTIMAN SEN² and
S RAMASESHA^{1*}

¹Solid State & Structural Chemistry Unit, and

²Centre for Theoretical Sciences, Indian Institute of Science,

Bangalore 560 012, India

e-mail: ramasesh@sscu.iisc.ernet.in

Abstract. One of the fascinating fields of study in magnetism in recent years has been the study of quantum phenomena in nanosystems. While semiconductor structures have provided paradigms of nanosystems from the stand point of electronic phenomena, the synthesis of high nuclearity transition metal complexes have provided examples of nano magnets. The range and diversity of the properties exhibited by these systems rivals its electronic counterparts. Qualitative understanding of these phenomena requires only a knowledge of basic physics, but quantitative study throws up many challenges that are similar to those encountered in the study of correlated electronic systems. In this article, a brief overview of the current trends in this area are highlighted and some of the efforts of our group in developing a quantitative understanding of this field are outlined.

Keywords. Quantum phenomena in magnetic systems; magnetic nano clusters; molecular magnets; nanoscale materials and structures.

1. Introduction

In recent years, synthesis of high nuclearity transition metal complexes in magnetic ground state has spurred interest in magnetism on a nanoscale¹. The synthesis of Mn₁₂ and Fe₈ clusters in $S = 10$ ground state and V₁₅ in the spin-half ground states have led to extensive study of quantum resonant tunnelling and quantum interference phenomena². Quantum resonant tunnelling manifests as plateaus in the magnetization vs magnetic field curves, with the width and location of plateaus being determined by the ramping speed of the magnetic field as well as the initial state. The quantum interference phenomena observed in the Fe₈ cluster are because the paths connecting the $M_s = +10$ and $M_s = -10$ could interfere in the presence of a magnetic field, leading to an oscillation in the tunnelling probabilities³.

All these systems consist of magnetic molecules which interact only weakly with each other. In Mn₁₂, each molecule is a cluster consisting of a core tetrahedron of four Mn⁴⁺ ions each with a spin of 3/2, and an outer crown consisting of eight Mn³⁺ ions each with spin 2. The exchange interactions are frustrated (see figure 1), leading to a high spin ground state with low-lying excitations also of high spin. Each molecule is a ferrimagnetic cluster with a ground state spin of 10. In these systems because of the rather complex exchange pathways which exist, it is difficult to predict *a priori* even the sign of the exchange constant, let alone its magnitude⁴. The Fe₈ cluster is shown in

*For correspondence

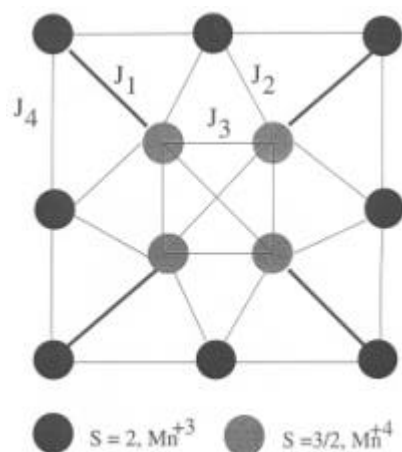


Figure 1. A schematic diagram of the exchange interactions between the Mn ions in the Mn_{12}Ac molecule. The interactions $J_1 = 215$ K and $J_2 = J_3 = 86$ K are antiferromagnetic, while $J_4 = 64.5$ K is ferromagnetic.

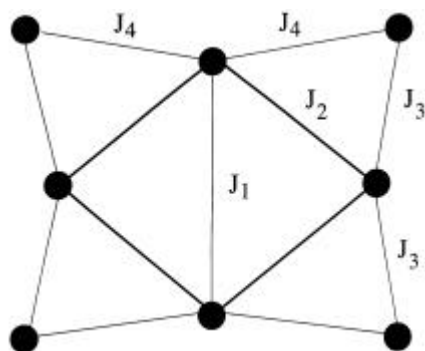


Figure 2. A schematic diagram of the exchange interactions between the Fe ions in the Fe_8 molecule.

figure 2. Each of the Fe ions has a spin of 2 and the ground state of the system has a total spin $S = 10$. All the exchange interactions in this system are expected to be antiferromagnetic, based on comparison with complexes containing similar exchange pathways. The structure of V_{15} is shown in figure 3. Structural and related studies on the cluster indicate that within each hexagon, there are three alternating exchanges $J \approx 800$ K which are the strongest in the system, and they define the energy scale of the problem. Besides, there are weaker exchange interactions between the spins involved in the strong exchange and also with the triangle spins which lie between the hexagons. All the exchange interactions are antiferromagnetic in nature. The exchange pathways and their strengths⁵ are also shown in figure 3. What is significant in the cluster is the fact that the spins in the triangle do not experience direct exchange interactions of any significance.

In the case of the Mn_{12} cluster, while the ground state spin as well as the lowest excitation gap is established experimentally, it is not at all clear what the magnitude and sign of the exchange interactions in the cluster are. In an earlier study⁶, in order to

one magnetization state to another is very small unless the sweeping frequency is so low that it is comparable to the matrix element connecting the two states. In V_{15} , a pair of doublets and a quartet formed from mainly the triangle spins are split off from the rest of the spectrum and the plateaus arise due to transition from the doublet to the triplet as the magnetic field is ramped.

In recent years, there have been many model calculations which illustrate such steps in the M vs H curves^{12,13}. These models involve either the presence of a transverse magnetic field, or higher order spin couplings which lead to a term of the type $c(\hat{S}_x^4 + \hat{S}_y^4)$ allowed by the symmetry of the cluster. However, most of these calculations have been restricted to the Landau–Zener two-level treatment within the spin-10 manifold. Besides, there also exists experimental evidence for low-lying excited states of $S \neq 10$ which lie within the $S = 10$ ground state manifold. Earlier studies have also ignored these states without any *a priori* justification. In contrast, we have carried out an exact calculation of the low-lying states of a $Mn_{12}Ac$ cluster using a Heisenberg spin model. We find that the symmetry of the excited states which lie within about ~ 100 K of the ground state are such as to prevent any admixture through a perturbation that does not change the C_4 symmetry of the cluster. Hence, it is sufficient to consider the 21 states belonging to the $S = 10$ ground state manifold in a low-temperature study. We have studied simultaneous quantum tunnelling amongst these low-lying states by setting up a Hamiltonian in this subspace of states which includes, besides the multipolar spin–spin interactions and a transverse magnetic field, different gyromagnetic ratios for the core and crown spins. This last interaction is reasonable to introduce because of the different environments around the core and crown spins (as confirmed by ESR experiments¹⁴). We have then evolved an initial state, which is taken to be the ground state with a specific value of M_S (the z -component of the total spin) in the absence of the magnetic field, by using the time-dependent formulation of the problem in the restricted subspace. The V_{15} cluster is far more amenable to rigorous quantum mechanical analysis because of the much smaller Fock space ($\approx 33,000$ dimensional) spanned by the unpaired spins of the system. A quantitative study of these systems requires that at least the low-lying states of the full spin-Hamiltonian is evolved in time, quantum mechanically as the external magnetic field is ramped with time as is done in experiments. In this article, we report our studies on the resonant tunnelling of magnetization in V_{15} by following the evolution of magnetization, as a function of the time-dependent magnetic field, at different temperatures. The low-lying states are obtained by solving the exchange Hamiltonian corresponding to all the spins of the system. The temperature dependence is introduced in the Hamiltonian via a spin–phonon interaction term which depends upon the thermal distribution of phonons and thermally averaging the magnetization over the low-lying states, after each of these states are independently evolved. We find that this model reproduces, quantitatively, all the experimental features⁵ associated with quantum resonant tunnelling in V_{15} .

2. Model Hamiltonian and computation details

The model Hamiltonian employed in these studies is the isotropic exchange Hamiltonian involving exchange interactions between nearest neighbours,

$$\hat{H} = \sum_{\langle ij \rangle} J_{ij} \hat{s}_i \cdot \hat{s}_j, \quad (1)$$

where the exchange interaction J_{ij} takes the values dictated by experimental studies of structure and magnetic properties. The total dimensionality of the Fock space of the cluster is given by

$$D_F = \prod_1^n (2S_i + 1), \quad (2)$$

where n is the total number of spins in the cluster and S_i is the spin on each cluster. In the case of Mn_{12} cluster consisting of eight spin-2 ions and four spin-3/2 ions, the Fock space dimensionality is a hundred million. Specialising to given total M_S leads to Hilbert space dimensionalities, which are lower than the Fock space dimensionality. In the case of the Mn_{12} cluster the $M_S = 0$ space has a dimensionality of over eight million (8,581,300).

The major challenge in exact computation of the eigenvalues, and properties of these spin clusters lies in handling such large bases and the associated matrices. While the dimensions look overwhelming, the matrices that represent the operators in these spaces are rather sparse. Usually, the number of nonzero elements in a row is of the order of the number of exchange constants in the Hamiltonian. This sparseness of the matrices allows one to handle fairly large systems. However, in the case of spin problems, generating the basis states and using the symmetries of the problem is nontrivial. The isotropic exchange Hamiltonians conserve total spin, S , besides the z -component of the total spin, M_S . Furthermore, the geometry of the cluster also leads to spatial symmetries which can often be exploited. The simplest way of generating bases functions which conserve total spin is the valence bond (VB) method that employs the Rumer–Pauling rule¹⁵. It is quite easy to generalize the Rumer–Pauling rules to a cluster consisting of objects with different spins to obtain states with desired total spin, S . However, setting-up the Hamiltonian matrix in such a basis can be computationally intensive since the exchange operators operating on a “legal” VB diagram (diagram that obeys Rumer–Pauling rules) could lead to “illegal” VB diagrams and resolving these “illegal” VB diagrams into “legal” diagrams would present the major bottle-neck. Indeed, the same difficulty is encountered when spatial symmetry operators operate on a VB function¹⁶. Thus, the extended VB methods are not favoured whenever one wishes to apply it to a motley collection of spins or when one wishes to exploit some general spatial symmetries that may exist in the cluster.

Usually, in frustrated spin systems, it is important to partition the spaces into different total spin spaces because of the usually small energy gaps between total spin states which differ in S by unity. To avoid the difficulties involved in working with total spin eigenfunctions, we exploit parity symmetry in the systems. The parity operation involves changing the z -component of all the spins in the cluster from M_{S_i} to $-M_{S_i}$. There is an associated phase factor with this operation given by $(-1)^{S_{tot} + \sum_i S_i}$. The isotropic exchange operator remains invariant under this operation. If this symmetry is employed in the $M_S = 0$ subspace, the subspace is divided into “even” and “odd” parity spaces depending upon the sign of the character under the irreducible representation of the parity group. The space which corresponds to even (odd) total spin is called the even (odd) parity space. Thus, employing parity allows partial spin symmetry adaptation which separates successive total spin spaces, without introducing the complications encountered in the VB bases. However, the VB method can lead to complete factorization of the spin space leading to smaller complete subspaces.

In the Mn_{12} cluster, besides spin symmetries, there also exists spatial symmetries. The topology of the exchange interaction leads to a C_4 point group symmetry. This point group appears at first site to present difficulties because the characters in the irreducible representation are in some cases complex. This could lead to complex bases functions. This, however, can be avoided by recognizing that in the C_n group, states with wavevectors k and $-k$ are degenerate in the absence of an external magnetic field. We can therefore construct a linear combination of the k and $-k$ states which is real. The symmetry representations in the C_4 group would then correspond to the labels A, B and E , with the characters in the E representation given by $2\cos(rk)$ under the symmetry operation C_4^r , with $k = \frac{\pi}{4}$. The parity operation commutes with the spatial symmetry operations and the full point group of the system would then correspond to the direct product of the two groups. Since both parity and spatial symmetries can be easily incorporated in a constant M_S basis, we do not encounter the difficulties endemic to the VB theory. In Fe_8 system, symmetry adaptation is straightforward although it is not critical. The same is true of the V_{15} system.

The generation of the complete basis in a given Hilbert space requires a simple representation of a state on the computer. This is achieved by associating with every state a unique integer. In this integer, we associate n_i bits with spin s_i , such that n_i is the smallest integer for which $2^{n_i} \leq (2s_i + 1)$. In the integer that represents the state of the cluster, we ensure that these n_i bits do not take values which lead to the n_i bit integer value exceeding $(2s_i + 1)$. For each of the allowed bit states of the n_i bit integer, we associate an M_{S_i} value between $-s_i$ and s_i . For a spin cluster of n spins, we scan all integers of bit length $N = \sum_{i=1}^n n_i$ and verify if it represents a basis state with the desired M_S value. Generation of the bases states is usually a very fast step, computationally. Generating the basis as an ordered sequence of integers that represent them also allows for rapid generation of the Hamiltonian matrix elements as will be seen later.

Symmetrization of the basis by incorporating parity and spatial symmetries involves operation on the constant M_S basis by the symmetry operators. Since spatial symmetry operators exchange the positions of equivalent spins, every spatial symmetry operator operating on a basis function generates another basis function. Every symmetry operator can be represented by a correspondence vector whose i th entry gives the state that results from operating on the i th state by the chosen operator. This is also true for the parity operator, in the $M_S = 0$ subspace. The symmetry combinations can now be obtained operating on each state by the group theoretic projection operator,

$$\hat{P}_{\Gamma_i} = \frac{1}{h} \sum_R \mathbf{c}_{\Gamma_i(R)} \hat{R}, \quad (3)$$

on each of the basis states. Here Γ_i is the i th irreducible representation, \hat{R} is the symmetry operation of the group and $\mathbf{c}_{\Gamma_i(R)}$ is the character under \hat{R} in the irreducible representation Γ_i . The resulting symmetrized basis is overcomplete. The linear dependencies can be eliminated by a Gram–Schmidt orthonormalization procedure. However, in most cases, ensuring that a given basis function does not appear more than once in a symmetrized basis is sufficient to guarantee linear independence and weed out the linearly dependent states. A good check on the procedure is to ensure that the dimensionality of the symmetrized space agrees with that calculated from the traces of the reducible representation obtained from the matrices corresponding to the symmetry

operators. Besides, the sum of the dimensionalities of the symmetrized spaces should correspond to the dimensionality of the unsymmetrized Hilbert space.

Generation of the Hamiltonian matrix is rather straightforward and involves operation of the Hamiltonian operator on the symmetry adapted basis. This results in the matrix \mathbf{SH} , where \mathbf{S} is the symmetrization matrix representing the operator \hat{P}_Γ and \mathbf{H} is the matrix whose elements h_{ij} are defined by

$$\hat{H} |i\rangle = \sum_j h_{ij} |j\rangle. \quad (4)$$

The states $\{i\}$ correspond to the unsymmetrized basis functions. The Hamiltonian matrix in the symmetrized basis is obtained by right multiplying the matrix \mathbf{SH} by \mathbf{S}^\dagger . The symmetric Hamiltonian matrix is stored in the sparse matrix form and the matrix eigenvalue problem is solved using the Davidson algorithm. Computation of the properties is easily done by transforming the eigenstate in the symmetrized basis into that in the unsymmetrized basis. Since the operation by any combination of spin operators on the unsymmetrized basis can be carried out, all relevant static properties in different eigenstates can be obtained quite simply.

We explicitly obtain the time evolution of the system by solving the time-dependent Schrödinger equation,

$$i\hbar \frac{d\mathbf{y}}{dt} = \hat{H}(t)\mathbf{y}. \quad (5)$$

The time dependence in the Hamiltonian arises because we increase the applied magnetic field in a chosen time dependent fashion. We assume the system to be in the appropriate initial state for e.g. in case of Mn_{12} we start with $S = 10$, $M_S = -10$ (all-spins-down state) at time $t = 0$. This is the initial state which is time evolved according to the equation

$$\mathbf{y}(t + \Delta t) = \exp(-i\hat{H}(t + (\Delta t/2)\Delta t/\hbar)\mathbf{y}(t). \quad (6)$$

The evolution is carried out by explicit diagonalization of the Hamiltonian matrix $\mathbf{H}(t + (\Delta t/2))$, and using the resulting eigenvalues and eigenvectors to evaluate the matrix of the time evolution operator $\exp(-i\hat{H}(t + (\Delta t/2)\Delta t/\hbar)$. Since the Hamiltonian matrix is in a truncated basis of 21 eigenstates of the magnetic cluster, it is possible to repeatedly carry out the time evolution in small time steps of size Δt . Each calculation typically involves time evolving the initial state by four million time steps. At each time step we calculate the magnetization of the state by obtaining the expectation value $\langle S_z \rangle$

3. Low-lying states of clusters

We have solved the exchange Hamiltonian exactly for the Mn_{12} , Fe_8 and V_{15} clusters using the method mentioned in the previous section. We have obtained the eigenvalues and various properties of the eigenstates such as spin densities and spin-spin correlation functions for these clusters¹⁷. In what follows, we will discuss these in detail.

3.1 $Mn_{12}Ac$ cluster

In figure 1 we show the geometry and the exchange parameters for this cluster. The crystal structure suggests that the exchange constant J_1 is largest and antiferromagnetic in nature¹⁸. Based on magnetic measurements, it has been suggested that J_1 has a magnitude of 215 K. Other magnitudes and signs of the other exchange constants are based on comparisons with manganese systems in smaller clusters¹⁸. It has been suggested that the exchange constant J_2 and J_3 are antiferromagnetic and have a magnitude of about 85 K. However, for the exchange constant J_4 , there is no concrete estimate, either of the sign or of the magnitude. In an earlier study the Mn^{III} - Mn^{IV} pair with the strongest antiferromagnetic exchange constant was replaced by a fictitious spin- $\frac{1}{2}$ object⁶ and the exchange Hamiltonian of the cluster solved for three different sets of parameters. It was found that the ordering of the energy levels were very sensitive to the relative strengths of the exchange constants. In these studies, J_4 was set to zero and the low-lying excited states were computed. Besides, only states with spin S upto ten could be obtained because of the replacement of the higher spin ions by the fictitious spin- $\frac{1}{2}$ object.

In our calculation, we have dealt with all the magnetic ions in the cluster and using symmetry, we have factored the $M_S = 0$ Hilbert space into the six symmetry subspaces. We have obtained low-lying eigenstates in each of these sectors and determined the total spin of the state by explicitly computing the expectation value of the \hat{S}^2 operator in the state.

Our results for the low-lying states are shown in table 1. We note that none of the three sets of parameters studied using an effective Hamiltonian, gives the correct ground and excited states, when an exact calculation is performed. It appears that setting the exchange constant J_4 to zero, cannot yield an $S = 10$ ground state (table 1, cases A, B and C). When J_3 is equal to or slightly larger than J_2 (cases A and B, table 1), we find a singlet ground state, unlike the result of the effective Hamiltonian in which the ground state has $S = 8$ and $S = 0$ respectively. The ground state has spin $S = 6$, when J_3 is slightly smaller than J_2 (case C, table 1). In all these case, the first few low-lying states are found to lie within 20 K of the ground state.

When we use the parameters suggested by Chudnovsky¹⁹ (case D, table 1), we obtain an $S = 10$ ground state separated from an $S = 9$ first excited state by 223 K. This is followed by another $S = 9$ excited state at 421 K. Only when the exchange constant J_4 is sufficiently strongly ferromagnetic (case E, table 1), do we find an $S = 10$ ground state with an $S = 9$ excited state separated from it by a gap of 35 K, which is close to the experimental value²⁰. The second higher excited state has $S = 8$, and is separated from the ground state by 62 K.

We have explored the parameter space a little further by varying J_3 and J_4 , to see the effect of these exchange constants on the ordering of the energy levels. We find that for $|J_3| = |J_4|$ and J_3 is antiferromagnetic but J_4 is ferromagnetic, and the ground state is always $S = 10$ (table 2, cases C, D and E); the first and second excited states are $S = 9$ and $S = 8$ respectively. The lowest excitation gap decreases slowly with increasing magnitude of the exchange constants.

We find that the spin of the ground state is very sensitive to J_4 , for a fixed value of J_3 . In the case where J_4 is weakly ferromagnetic (table 2, case B), we obtain an $S = 0$ ground state, and when J_4 is weakly antiferromagnetic we obtain an $S = 4$ ground state (table 2, case A). This shows that frustrations play a dominant role. If J_3 is also made ferromagnetic, the role of frustration is considerably reduced.

Table 1. Low-lying states of $Mn_{12}Ac$, relative to the ground state for the parameters in question. Entries in parentheses in cases A, B and C correspond to the effective Hamiltonian results of Sessoli *et al*.⁶ Case D corresponds to the parameters suggested by Chudnovsky¹⁹. The parameters corresponding to different cases are: case (A) $J_1 = 225$ K, $J_2 = 90$ K, $J_3 = 90$ K, $J_4 = 0$ K; case (B) $J_1 = 225$ K, $J_2 = 90$ K, $J_3 = 93.8$ K, $J_4 = 0$ K; case (C) $J_1 = 225$ K, $J_2 = 90$ K, $J_3 = 86.2$ K, $J_4 = 0$ K; case (D) $J_1 = 215$ K, $J_2 = 85$ K, $J_3 = -85$ K, $J_4 = -45$ K; case (E) $J_1 = 215$ K, $J_2 = 85$ K, $J_3 = 85$ K, $J_4 = -64.5$ K. All the energies are in K.

Case A			Case B			Case C			Case D			Case E		
State	S	E(K)	State	S	E(K)	State	S	E(K)	State	S	E(K)	State	S	E(K)
^e B	0	0.0	^e B	0	0.0	^e B	6	0.0	^e A	10	0.0	^e A	10	0.0
	(8)		(0)	(10)										
^o E	1	10.8	^o E	1	16.2	^o E	1	15.5	^o E	19	223	^o E	9	35.1
	(9)	(6.4)	(8)	(1.4)	(8)			(2.7)						
	(10)													
^o B	1	19.8	^o B	1	20.0	^o B	1	19.6	^o B	9	421.2	^o B	8	62.1
	(0)	(6.8)				(9)		(5.0)						
^e A	2	24.7	^e A	2	30.5	^e A	2	23.8	^o B	9	425.1	^o E	7	82.4
^o E	3	39.0	^e B	4	58.4	^o E	1	28.8	^e B	8	439.5	^e A	6	99.7
^e E	2	49.9	^e E	2	60.9	^e B	6	53.6	^e B	8	443.7	^e B	0	102.0
^e B	4	57.1	^o A	3	64.3	^e B	6	54.4	^e B	8	458.1	^e A	2	121.0
^e B	8	57.8	^e E	2	80.0	^e B	8	57.2	^o A	11	573.4	^o B	1	133.3
^e B	2	57.8	^o A	3	88.1	^e E	2	63.0	^o E	9	583.8	^e E	2	177.1
^o B	3	78.4	^e A	6	88.3	^o A	3	77.0	^e E	8	632.8	^o A	3	211.3
^o B	3	86.8	^o B	3	112.8	^o B	3	85.3	^o A	9	640.5	^e A	3	220.8
^e A	6	105.7	^o B	5	114.6	^e E	2	86.1	^e E	8	658.3	^e E	4	249.9
^o B	3	113.4	^o B	5	158.4	^e A	6	97.1	^e A	8	767.1	^o B	5	278.5
^e E	4	117.3	^o A	1	165.2	^e A	6	98.2	^e B	8	807.6	^o A	7	332.1
^o B	5	154.2	^o A	1	181.6	^o B	3	112.2	^e A	8	815.8	^o A	7	340.8

Table 2. Low-lying states of Mn₁₂Ac. The parameters corresponding to different cases are: case (A) $J_1 = 215$ K, $J_2 = 85$ K, $J_3 = 85$ K, $J_4 = 45$ K; case (B) $J_1 = 215$ K, $J_2 = 85$ K, $J_3 = 85$ K, $J_4 = -45$ K; case (C) $J_1 = 215$ K, $J_2 = 85$ K, $J_3 = 64.5$ K, $J_4 = -64.5$ K; case (D) $J_1 = 215$ K, $J_2 = 85$ K, $J_3 = 85$ K, $J_4 = -85$ K; case (E) $J_1 = 215$ K, $J_2 = 85$ K, $J_3 = 45$ K, $J_4 = -45$ K. All the energies are in K.

State	Case A			Case B			Case C			Case D			Case E		
	S	E(K)	State												
^e B	4	0.0	^e B	0	0.0	^e A	10	0.0	^e A	10	0.0	^e A	10	0.0	^e A
^e A	4	9.1	^o E	1	12.3	^o E	9	73.7	^o E	9	67.7	^o E	9	80.1	^o E
^o E	3	9.4	^e A	2	22.9	^e B	8	135.1	^e B	8	121.2	^e B	8	149.8	^e B
^e B	4	18.2	^o B	1	27.6	^o E	7	186.1	^o E	7	165.2	^e A	8	191.0	^e A
^e A	2	32.4	^o E	3	28.9	^e A	8	196.0	^e A	6	201.2	^o E	7	210.0	^o E
^o B	5	49.4	^e B	4	34.1	^e A	6	227.8	^e A	8	206.5	^e A	6	260.0	^e A
^e A	6	50.0	^e A	10	36.5	^e B	4	283.5	^e B	4	247.7	^e B	4	329.8	^e B
^e E	4	55.4	^e B	8	37.8	^o B	1	323.0	^o B	1	282.5	^o B	9	346.8	^o B
^o A	3	68.2	^e E	2	67.2	^e E	2	364.0	^e E	2	330.2	^o B	9	370.7	^o B
^o A	3	70.2	^o A	3	100.1	^o A	3	391.8	^o A	3	365.2	^o B	1	515.8	^o B
^o B	3	71.4	^o A	3	119.5	^o A	3	401.6	^o A	3	375.0	^e E	8	400.3	^e E
^o A	3	76.6	^e A	4	140.0	^e E	4	420.6	^e E	4	401.9	^e E	2	413.8	^e E
^e B	2	255.2	^o B	3	161.8	^o B	9	426.3	^o B	11	421.0	^o A	5	424.2	^o A
^e B	2	257.2	^o B	5	172.8	^o B	5	434.9	^o B	5	425.5	^o A	3	432.5	^o A

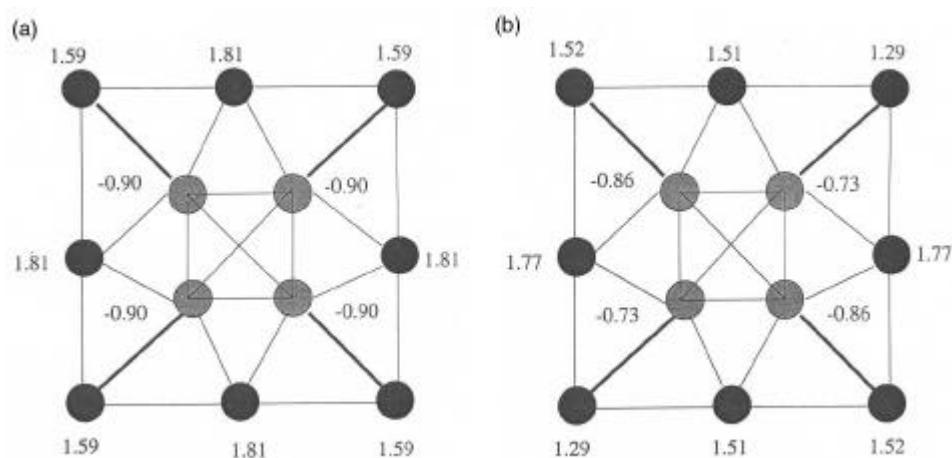


Figure 4. Spin density of Mn_{12}Ac for parameter values: $J_1 = 215 \text{ K}$, $J_2 = 85 \text{ K}$, $J_3 = 85 \text{ K}$ and $J_4 = -64.5 \text{ K}$. (a) Spin density for ground state ($S = 10$, $M_S = 10$). (b) Spin density for 1st excited state ($S = 9$, $M_S = 9$).

In figures 4a and b, we show the spin density²¹ for the Mn_{12} cluster in the ground state for the $S = 10$, $M_S = 10$ state. While the manganese ions connected by the strong antiferromagnetic exchange show opposite spin densities, it is worth noting that the total spin density on these two ions is 0.691, well away from a value of 0.5 expected, if these ions were indeed to form a spin $-\frac{1}{2}$ object. We also note that the spin density at the manganese ion in the middle of the crown is much larger than that at the corners. The spin density in the excited state $S = 9$, $M_S = 9$, also has similar distribution, although in this state, the symmetry of the spin Hamiltonian is apparently broken (figure 4b). The corner ions in the crown no longer have the same spin density and, in fact, a pair of opposite corner ions have larger spin density than on ions in the middle of the crown. However, since this state is doubly degenerate, there is another state in which the spin densities are related to the spin densities of this state by a ninety degree rotation. In any experiment involving this state, only an arbitrary linear combination of the two spin densities is observed. Note also that the large differences in the spin densities for the closely lying excited states are an indication of the large degree of spin frustration in the system.

The small energy gap (35 K) between the $S = 10$ ground state and the $S = 9$ lowest excited state seems to indicate that, if the g factors of the Mn ions in the core and crown are different, then an applied magnetic field should mix these spin states. Such a mixing would then be reflected in the quantum resonance tunnelling experiments. However, it appears that the experiments are well-described by the $S = 10$ state alone. This is what we should expect from the symmetry of the two low-lying states. We note that the ground state has A symmetry while the lowest excited state has an E symmetry. These two states cannot be mixed by any perturbation that retains the C_4 symmetry of the cluster.

3.2 Fe_8 cluster

The Fe_8 cluster is shown in figure 2. Each of the Fe ions has a spin of 2 and the ground state of the system has a total spin $S = 10$, with the $S = 9$ excited state separated from it

by about 20 K. All the exchange interactions in this system are expected to be antiferromagnetic. While the structure of the complex dictates that the exchange interaction J_2 along the back of the butterfly should be considerably small in comparison with the interaction J_1 across the wing²², in earlier studies it was reported that such a choice of interaction parameters would not provide a $S = 10$ ground state⁷.

We have carried out exact calculations of the eigenstates of the Fe_8 cluster using three sets of parameters. In two of these cases, J_2 is very much smaller than J_1 . We find that in all these cases, the ground state has a spin $S = 10$ and the lowest excited state has spin, $S = 9$. One of the main difference we find amongst the three sets of parameters is in the energy gap to the lowest excited state (table 3). For the set of parameters used in the earlier study, this gap is the lowest at 3.4 K. For the parameter sets 1 and 3⁸ this gap is respectively 13.1 K and 38.0 K. While in cases 1 and 2, the second excited state is an $S = 8$ state, in case 3, this state also has spin 9.

The spin densities in all the three cases for both the ground and the excited state are shown in figures 5a to f. The spin densities in all cases are positive at the corners. In cases 1 and 2, the spin density on the Fe ion on the backbone is positive and negative on the remaining two Fe sites²³ However, in case 3, the negative and positive spin density sites for Fe ions in the middle of the edges is interchanged. This is perhaps due to the fact that in cases 1 and 2, the exchange constant J_3 is less than J_4 , while in case 3, this is reversed. Thus, a spin density measurement can provide relative strengths of these two exchange constants. In all the three case, the difference between the spin densities in the ground and excited states is that the decrease in the spin density in the excited state is mainly confined to the corner Fe sites.

The Fe_8 cluster is quite different from the Mn_{12} cluster in the following sense. In the Fe_8 cluster, we have excited states of spin $S = 8$ and $S = 9$ which have the same symmetry as that of the $S = 10$ ground state. Furthermore, the total splitting of the ground state due to the anisotropic terms arising in the system due to spin-dipolar interactions is larger than the energy gaps with the $S = 8$ and $S = 9$ states of the same spatial symmetry as the ground state. Thus, if the g factors of the Fe ions on the backbone of the butterfly are different from those on the wings, then an applied magnetic field could lead to mixing between the different spin states. We expect this to provide an additional mechanism for quantum resonance tunnelling in the Fe_8 cluster.

3.3 V_{15} cluster

The simplest cluster to study is the V_{15} cluster, since each of the ions has a spin of half. The interesting aspect of the V_{15} cluster is that the three spins sandwiched between the

Table 3. Energies (in units of K) of a few low-lying states in Fe_8 . The exchange constants corresponding to the various cases are: case (A) $J_1 = 25$ K, $J_2 = 150$ K, $J_3 = 30$ K, $J_4 = 50$ K; case (B) $J_1 = 153$ K, $J_2 = 180$ K, $J_3 = 22.5$ K, $J_4 = 52.5$ K; case (C) $J_1 = 30$ K, $J_2 = 195$ K, $J_3 = 52.5$ K, $J_4 = 22.5$ K.

Case A			Case B			Case C		
State	S	$E(\text{K})$	State	S	$E(\text{K})$	State	S	$E(\text{K})$
${}^e\text{A}$	10	0.0	${}^e\text{A}$	10	0.0	${}^e\text{A}$	10	0.0
${}^o\text{B}$	9	13.1	${}^o\text{B}$	9	3.4	${}^o\text{A}$	9	39.6
${}^o\text{A}$	9	26.1	${}^e\text{A}$	8	10.2	${}^o\text{B}$	9	54.2
${}^e\text{A}$	8	27.3	${}^o\text{B}$	7	20.1	${}^o\text{B}$	9	62.4

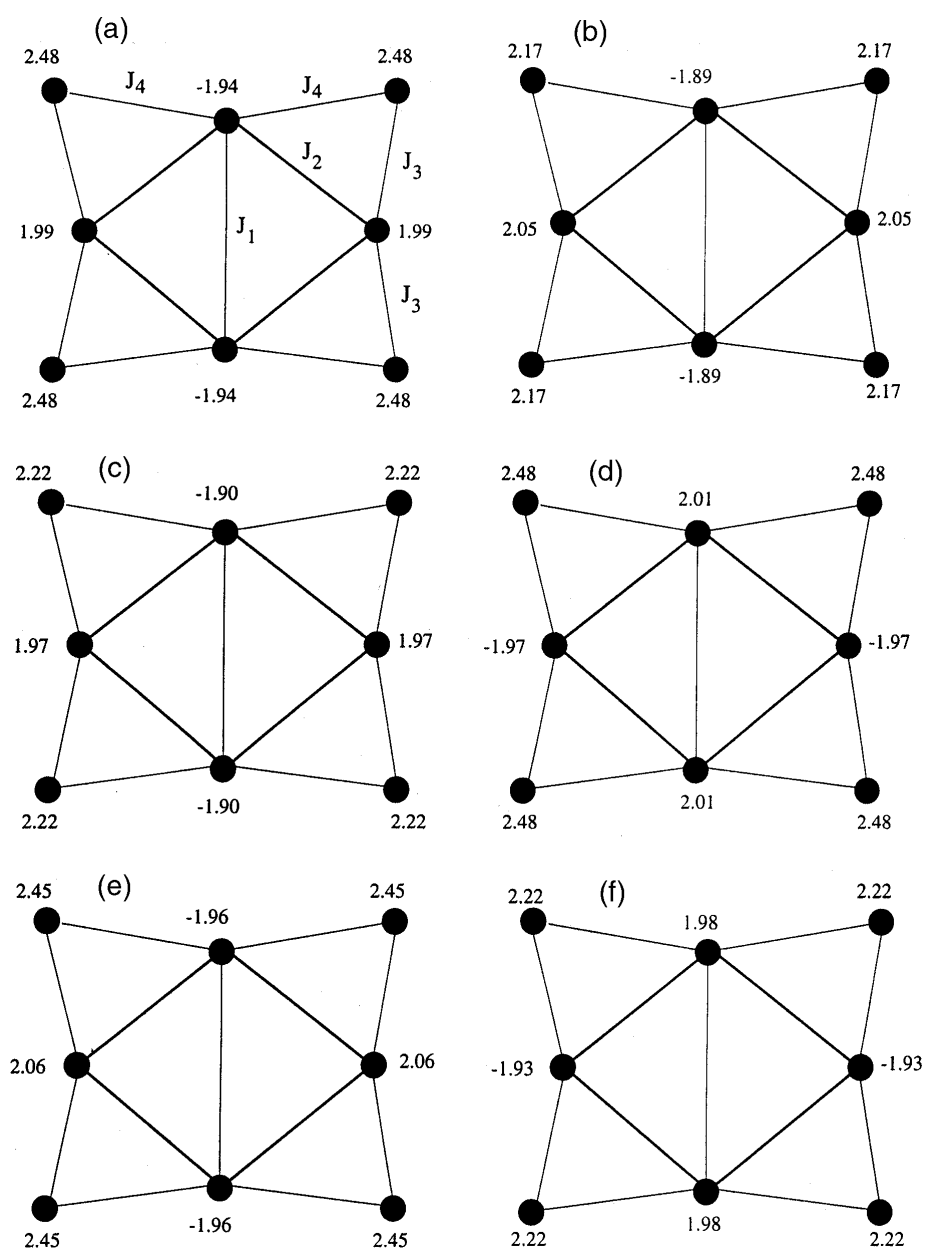


Figure 5. Spin density of Fe_8 for parameter values: $J_1 = 25 \text{ K}$, $J_2 = 150 \text{ K}$, $J_3 = 30 \text{ K}$, $J_4 = 50 \text{ K}$. (a) Spin density for ground state ($S = 10$, $M_s = 10$). (b) Spin density for 1st excited state ($S = 9$, $M_s = 9$). Spin density of Fe_8 for $J_1 = 153 \text{ K}$, $J_2 = 180 \text{ K}$, $J_3 = 22.5 \text{ K}$, $J_4 = 52.5 \text{ K}$ parameter values. (c) Spin density for ground state ($S = 10$, $M_s = -10$). (d) Spin density for 1st excited state ($S = 9$, $M_s = -9$). Spin density of Fe_8 for $J_1 = 30 \text{ K}$, $J_2 = 195 \text{ K}$, $J_3 = 52.5 \text{ K}$, $J_4 = 22.5 \text{ K}$ parameter values. (e) Spin density for ground state ($S = 10$, $M_s = 10$). (f) Spin density for 1st excited state ($S = 9$, $M_s = 9$).

hexagons (figure 3) have no direct spin–spin interactions. All the interactions shown in figure 3 are antiferromagnetic and the spin system is frustrated. Eigenstates of this system consists of eight states corresponding to the triangle spins which have split off from the rest of the spectrum. We find the effective Hamiltonian is given by,

$$H_{\text{sp-sp}} = \mathbf{e} + \mathbf{a}(S_1 \cdot S_2 + S_2 \cdot S_3 + S_3 \cdot S_1), \quad (7)$$

where $\mathbf{e} = -4.58590955$ and $\mathbf{a} = 0.0034373$, in units of the exchange J . This Hamiltonian reproduces the eight low-lying eigenstates of the full exchange Hamiltonian to numerical accuracy.

The spin density distribution in the $S = 1/2$, $M_S = 1/2$ ground and excited states as well as in the $S = 3/2$, $M_S = 3/2$ states is shown in figures 6a to c. We find that the spin densities on the hexagons are negligible. In the lowest $S = 1/2$ state, the triangle spins have both positive and negative spin densities, while the higher $S = 1/2$ state is characterized by positive and zero spin densities. This clearly implies that the exchange interactions felt by these spins is antiferromagnetic in nature. The $S = 3/2$, $M_S = 3/2$ states have almost equal spin densities at all three sites, nearly equal in value to that of the free spins. In fact, the total spin density in the $S = 1/2$ states is also nearly that of a free-electron spin and this suggests that describing the low-energy spectrum of this system by the triangle spin is quite appropriate.

4. Quantum tunnelling in Mn_{12}Ac cluster

To study quantum tunnelling in Mn_{12} we have considered the effective Hamiltonian defined over the $S = 10$ ground state of the cluster in the presence of an external magnetic field²⁴. The Hamiltonian is given by,

$$\hat{H} = -D\hat{S}_{z,\text{total}}^2 + c(\hat{S}_{x,\text{total}}^4 + \hat{S}_{y,\text{total}}^4) - g_{\text{crown}}\mathbf{H}(t) \cdot \hat{S}_{\text{crown}} - g_{\text{core}}\mathbf{H}(t) \cdot \hat{S}_{\text{core}}. \quad (8)$$

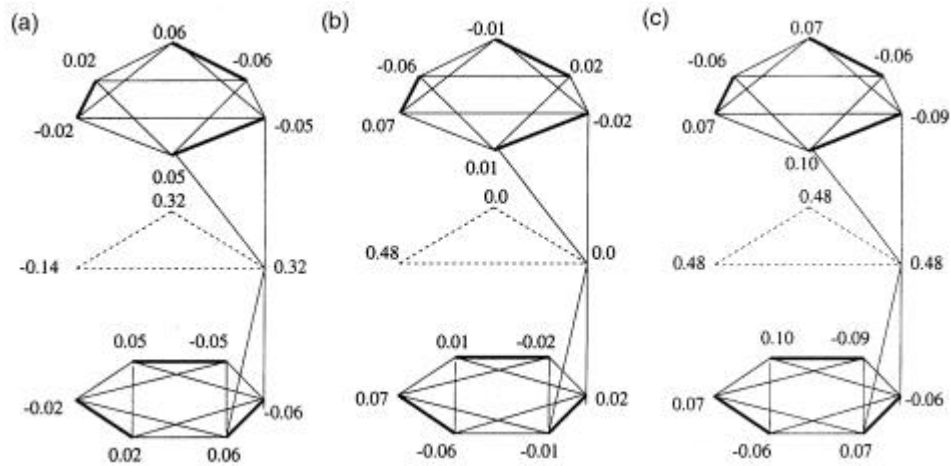


Figure 6. Spin density of V_{15} for $J_1 = 800$ K, $J_2 = 300$ K, $J_3 = 150$ K parameter values. (a) Spin density for ground state ($S = 0.5$, $M_S = 0.5$). (b) Spin density for 1st excited state ($S = 0.5$, $M_S = 0.5$). (c) Spin density for excited state ($S = 1.5$, $M_S = 1.5$).

Here D is the quadratic anisotropy factor, g_{crown} and g_{core} are the Landé g -factors for the crown and core spin respectively, and $\mathbf{H}(t)$ is the time-dependent magnetic field. We have chosen $D = 3.5 \times 10^{-3}$ and $c = 10^{-3}$ (in units of J_1) in accordance with the experimental values^{25,26}. We take $g_{\text{crown}} = 1.96$ and $g_{\text{core}} = 2.0$. The fourth-order anisotropy term allows transitions between states with $\Delta M_S = \pm 4$. To study the evolution of the magnetization as a function of the applied magnetic field, we start from an axial field equal to -1 (in units of J_1/\hbar) and then slowly increase it in steps till it equals $+1$.

The Hamiltonian matrix is set-up in the $M_S = 10$ subspace and the lowest energy state is obtained using the Davidson algorithm²⁷. We calculate the spin densities and the spin–spin correlation functions in this state. Using the spin–spin correlation functions, we have computed the expectation value of S_{total}^2 operator, from which we have confirmed the total spin of the state to be $S = 10$. We also compute the total spin density of the core and crown spins in this state. From the total spin and the spin density of the core and crown spins in the $M_S = 10$ state, using the spin ladder operators we obtain the spin densities in the core and crown of the cluster for all the allowed M_S values. These are later used in computing the magnetization response of the system.

We have carried out a systematic investigation of the dependence of the magnetization steps on the field sweep rate, the fourth order anisotropy term, and the presence of a transverse field.

It is useful to have an idea of the energy levels of the system as a function of the magnetic field. Figure 7 shows the energy levels of the Hamiltonian in (8) with a constant

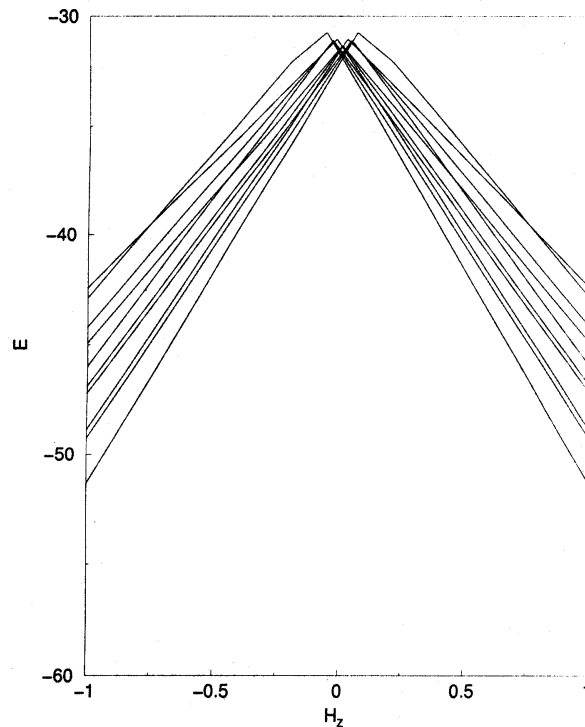


Figure 7. Energy spectrum of the Hamiltonian in (8) in the presence of a time-independent axial field. Only a few low-lying energy levels are shown.

axial magnetic field $\mathbf{H}(t) = H_z(t)\hat{z}$. For the field value $H_z = 0$, levels with opposite magnetizations $\pm M_S$ are degenerate; the energy spectrum is symmetric about $H_z = 0$. We can see from the figure that there are at least three values of the axial field where level crossings occur. Crossings occur around $H_z = \pm 0.13, \pm 0.43$ and ± 0.75 (in units of J_1/\hbar). When we sweep the field, we should expect to see jumps in the magnetization value in the neighborhood of these values of the field where the crossings occur; however the actual values of the fields where crossings occur depend on the fourth order anisotropy term. Besides, as we will see, the occurrence and widths of plateaus in the magnetization are strongly dependent on the field sweep rate. The number of plateaus and their locations and widths depend on the probability of tunnelling from one magnetization state to another. This probability increases when the time scale of sweeping matches with the time scale of tunnelling. In that case, the probability of staying in the same eigenstate is small; the state is scattered into another eigenstate which produces a step in the magnetization plot.

Following the field sweeping technique used by De Raedt *et al*¹³, we now study the behaviour of the magnetization as the field is changed with time. The magnetic field H_z is increased from -1 to 1 in steps of 5×10^{-4} (all in units of J_1/\hbar). At each value of the field, the state is evolved for 1000 time steps of size Δt . We have considered two different time step values given by $\Delta t = 0.01 \hbar/J_1$ and $0.1 \hbar/J_1$; thus each value of the field is kept fixed for a time equal to $10 \hbar/J_1$ and $100 \hbar/J_1$ respectively. The field sweep rate is given by $5 \times 10^{-7}/\Delta t$; we therefore have two sweep rates differing by a factor of 10. At each time step, the time evolved state is used to compute the magnetization M given by

$$M(t) = \langle \mathbf{Y}(t) | \hat{S}_{z, \text{total}} | \mathbf{Y}(t) \rangle. \quad (9)$$

The magnetization at each value of the field is then taken to be the average of the magnetization computed over all the time steps for which the field is held fixed.

In figure 8, we show the step behaviour of the magnetization with the applied field. The upper curve is for a time step equal to 0.1 (in units of \hbar/J_1), while the lower curve is for a time step of 0.01 . We observe jumps in the magnetization plot at field values of approximately $H_z = 0.13 J_1/\hbar$ and $0.33 J_1/\hbar$. Before the first jump in the magnetization the magnetization value remains almost constant at -10 . The reason why we do not see any jumps at the corresponding negative fields $H_z = -0.13 J_1/\hbar$ or $-0.33 J_1/\hbar$ is because at those field values, $M_S = -10$ continues to be the ground state. For positive field values, $M_S = +10$ is the ground state, and states with lower positive values of M_S successively come into resonance with the $M_S = -10$ state. We observe a remarkable thing that the magnetization value seems to saturate after a certain time evolution, but it never approaches the state with $M_S = 10$. We can argue that in our model the system can only gain or lose energy by interacting with the time-dependent field; there is no interaction with the environment through, for example, spin-phonon or nuclear spin-electron spin interactions which provide the mechanism for relaxation to the ground state. The $M_S = -10$ state tunnels to states with $0 \leq M_S < 10$, and to attain $M_S = 10$ state, the final state in the tunnelling process needs to relax to the ground state. So even for very large H_z the magnetization does not reach the saturation value in a finite time. However, the magnetization does reach a higher value for large fields if the sweep rate is lower, since there is more time to tunnel to the lowest energy states in that case. The inset of figure 8 shows the result obtained when the field is held fixed for a longer time equal to $200 \hbar/J_1$ corresponding to 2000 time steps of size $0.1 \hbar/J_1$ each. Note that the plateau in the inset

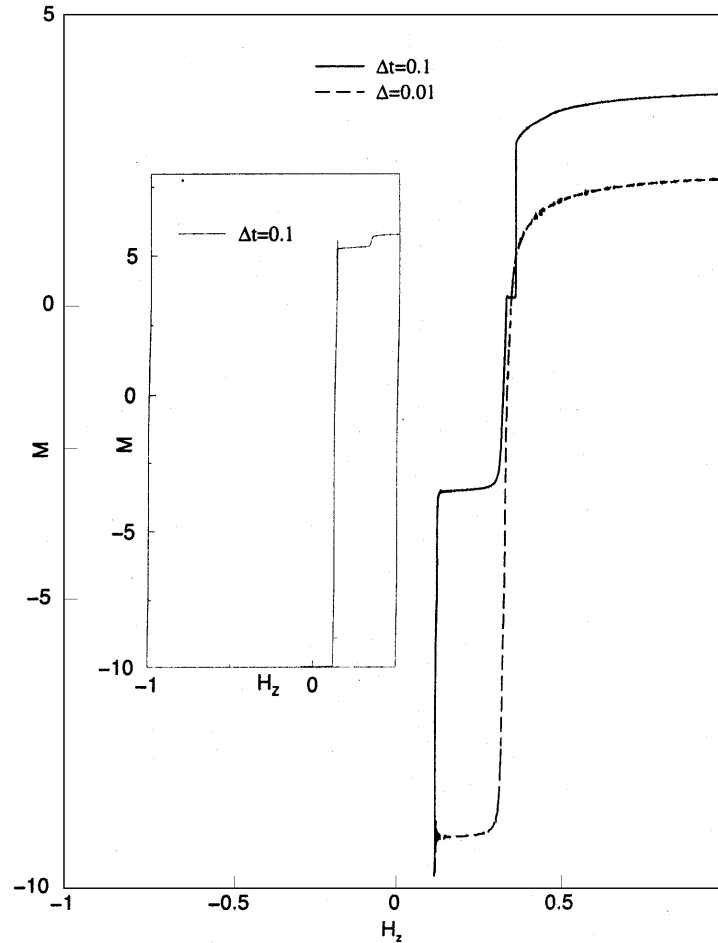


Figure 8. Evolution of magnetization at two different sweep rates. The upper curve is for a time step equal to 0.1 (in units of \hbar/J_1), while the lower curve is for a time step of 0.01. The inset shows the result obtained when the field is held fixed for a time equal to $200 \hbar/J_1$.

occurs at a different value of the magnetization compared to the plateaus in the two curves in the main figure where the sweep rates were faster. This is due to tunnelling to nearly degenerate states with different values of the magnetization.

5. Model for magnetization plateaus in V_{15}

We study the magnetization of V_{15} by following its evolution as a function of a time-dependent magnetic field at different temperatures²⁸. The low-lying states are obtained by solving the exchange Hamiltonian corresponding to all the spins of the system. A spin-phonon interaction is then introduced in the Hamiltonian. We thermally average the magnetization over the low-lying states after each of these states is independently evolved. We find that this model reproduces quantitatively most of the experimental

features found in the magnetization studies of V_{15} ⁵, without invoking *ad hoc* concepts such as a “phonon bottleneck”.

The exchange Hamiltonian of the cluster is solved by (7). The direct spin–spin interaction terms permitted by the C_3 symmetry are given by

$$H_{\text{dip}} = \mathbf{g}[(S_+^3 + S_-^3) + i(S_+^3 - S_-^3)]. \quad (10)$$

We have also introduced a coupling between the spin states of the cluster and the phonons. The spin-phonon interaction Hamiltonian which preserves the C_3 symmetry is phenomenologically given by²⁹

$$H_{\text{sp-ph}} = q(b + b^\dagger)[(S_+^2 + S_-^2) + i(S_+^2 - S_-^2) + (S_z^2 - \frac{1}{3}S^3)], \quad (11)$$

where q is the spin-phonon coupling constant, $b(b^\dagger)$ is the phonon annihilation (creation) operator, and $\hbar\mathbf{w}$ is the phonon frequency. For simplicity, we have assumed a single phonon mode although the molecule has various possible vibrational modes. The form of the interaction in (11) means that the phonons couple only to states with spin $-3/2$. We have restricted the dimensionality of the Fock space of the phonons to 15 considering the low temperatures of interest.

The evolution of the magnetization as a function of the magnetic field has been studied by using the total Hamiltonian H_{total} , given by

$$H_{\text{total}} = H_{\text{sp-sp}} + H_{\text{dip}} + H_{\text{sp-ph}} + \hbar\mathbf{w}(b^\dagger b + 1/2) + h_z(t)S_z + h_x(t)S_x, \quad (12)$$

where we have assumed that besides an axial field $h_z(t)$, a small transverse field $h_x(t)$ could also be present to account for any mismatch between the crystalline z -axis and the molecular z -axis. The numerical method involves setting up the Hamiltonian matrix in the product basis of the spin and phonon states $|i, j\rangle$, where $|i\rangle$ corresponds to one of the eight spin configurations of the three spins, and j varies from 0 to 14, corresponding to the fifteen phonon states retained in the problem. The values we have assigned to the different parameters are $\mathbf{g} = 10^{-3}$, $q = 10^{-4}$ and $\hbar\mathbf{w} = 1.25 \times 10^{-4}$, all in units of the exchange J (see figure 3).

To study the magnetization phenomena, we start with the direct product eigenstates of $H_{\text{sp-sp}}$ and $\hbar\mathbf{w}(b^\dagger b + 1/2)$, and independently evolve each of the 120 states \mathbf{y}_j by using the time evolution operator

$$\mathbf{y}(t + \Delta t) = \exp(-iH_{\text{total}}\Delta t/\hbar)\mathbf{y}(t). \quad (13)$$

The evolution is carried out in small time steps by applying the evolution operator to the state arrived at in the previous step. The magnetic field is changed step-wise in units of 0.015 T. At each value of the magnetic field, the system is allowed to evolve for 300 time steps of size Δt , before the field is changed to the next value. At every time step, the average magnetization $\langle M(t) \rangle$ is calculated as

$$\langle M(t) \rangle = \sum_{i=1}^8 \sum_{j=0}^{14} \frac{\exp(-\mathbf{b}w_i + h_z(t)m_i) \exp(-\mathbf{b}\hbar\mathbf{w}(j + 1/2))}{Z_{\text{spin}} Z_{\text{ph}}} \langle \mathbf{y}_{ij}(t) | \hat{S}_z | \mathbf{y}_{ij}(t) \rangle, \quad (14)$$

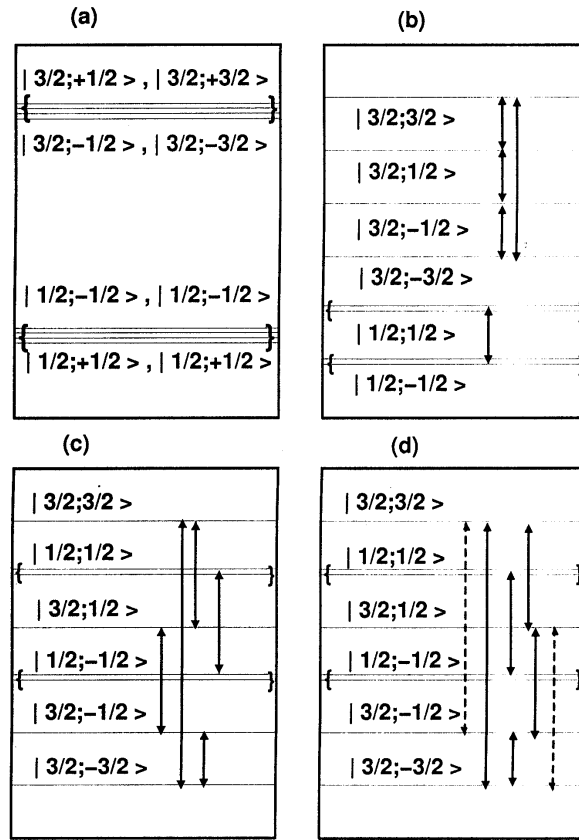


Figure 9. (a) Eigenstates of the effective spin Hamiltonian $H_{\text{sp-sp}}$ (b) Eigenstates in the presence of a moderate axial field. Arrows show the states connected by the dipolar terms and the transverse field. (c) is the same as (b) but in a stronger field, (d) describes the effect of spin-phonon terms (shown by arrows with broken lines) on (c).

where w_i and m_i are the eigenvalues and magnetizations of eigenstates of $H_{\text{sp-sp}}$, $\mathbf{b} = 1/k_B T$, Z_{ph} is the phonon partition function of $\hbar \omega (b^\dagger b + 1/2)$, and Z_{spin} is the partition function of $H_{\text{sp-sp}}$ in the presence of the axial magnetic field. In figure 9, we show the energy level ordering of the effective spin Hamiltonian and the effect of the magnetic field on the eigenvalue spectrum. We also show the couplings between various states brought about by the magnetic dipolar terms and the spin-phonon terms; note that the spin $-1/2$ and spin $-3/2$ states are not connected to each other by these terms.

In figure 10, we show the hysteresis plots of the system for different temperatures. We see that at low temperatures, the plateaus in the hysteresis plots are very pronounced. The width of transition from $\langle S_z \rangle = -0.5$ to -1.5 corresponds to 2.8 T which is in excellent agreement with the experimental value of 2.82 T⁵ assuming that $J = 800$ K. We also find that the plateau vanishes above a temperature of 0.9 K which is also in excellent agreement with the experimental value of 0.9 K⁵. The inset in figure 10 shows the temperature variation of the plateau width. We note that the plateau width falls off rapidly with temperature, and an exponential fit to $W = A \exp(-T/\Omega)$ (see figure 10) gives

the characteristic temperature Ω to be 0.2 K. This small value of Ω is because there are no large barriers between the different magnetization states in this system, unlike the high spin molecular magnets such as Mn_{12}^{30} . The width of the plateau as well as the field at which it occurs is very sensitive to the model parameters. We see in figure 11 that for the set of parameters corresponding to (a), both the width of the transition and the field of onset of the transition agree with experiments.

We also observe that when the field is swept more rapidly, there are additional plateaus at intermediate values of magnetization. For example, when the field sweep rate is increased by a factor of five compared to figure 10, we find a small plateau of width 0.03 T near $H=0.15$ T at a value of $\langle S_z \rangle = -0.375$. This is because near that field, some of the spin $-3/2$ states become degenerate in energy; subsequently, as the magnetic field is increased, the system stays locked in some of those states if the sweep rate is too high. This plateau vanishes on warming the system slightly.

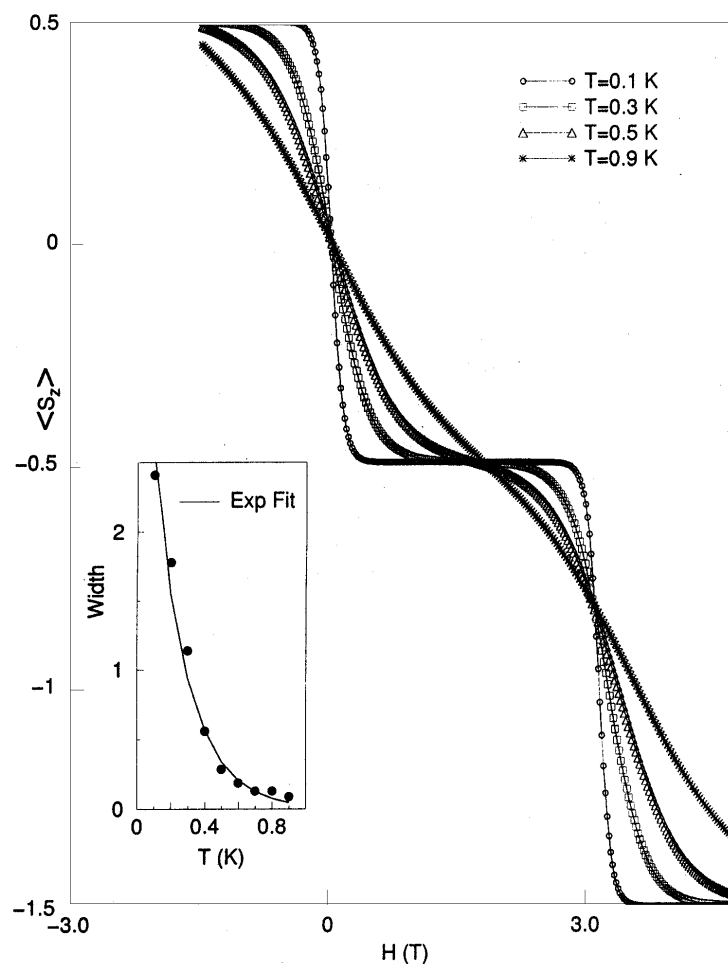


Figure 10. Plot of magnetization vs axial field at different temperatures. Inset shows plateau width as a function of temperature (full circles).

6. Dynamic magnetization oscillations

The energy level structure of the eigenstates of Hamiltonian in (8) are very similar to those encountered in the dynamic studies of two-level lattices. There has been considerable study of the two-level lattices in which Stark–Wannier effect and Bloch oscillations are observed^{31,32}. In the presence of oscillatory electric fields, population trapping³³ and dynamic localization³⁴ have also been observed. The aim of the present study is to see if these effects can also be observed in the Mn_{12} magnetic cluster in the presence of an oscillatory magnetic field³⁵.

As before the initial state in the time evolution is chosen to be the state with $S = 10$ and $M_S = -10$, which is the ground state, in the absence of the weak off-diagonal terms of H_{dip} . The angular frequency, ω of the axial field is varied between 10^{-1} and 10^{-3} radian- D/\hbar . The time evolution is carried out successively in steps $\Delta t = 0.1$ and the evolution is carried out over several periods of the applied field.

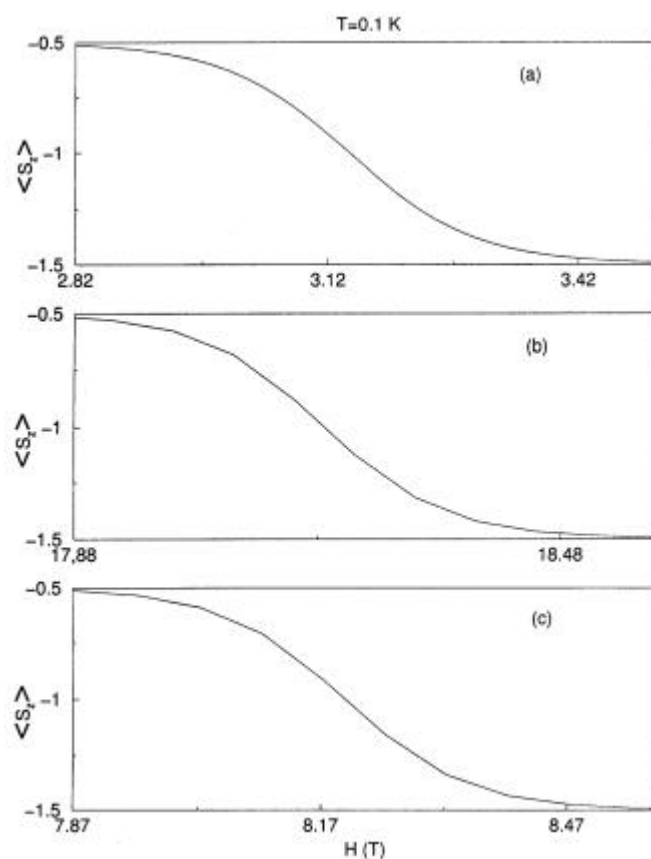


Figure 11. Comparison of the width of transition and the field of onset of transition from $\langle S_z \rangle = -0.5$ to -1.5 depending on different parameter values. (a) $J = 800$ K, $J_1 = 54.4$ K, $J_2 = 160$ K (b) $J = 800$ K, $J_1 = 150$ K, $J_2 = 300$ K⁵ (c) $J = 756$ K, $J_1 = 28.8$ K, $J_2 = 178.56$ K¹. Onset field values are 2.82 T, 17.88 T and 7.87 T respectively for parameters a, b and c. Experimental value of the field of onset of transition is 2.8 T.

In figure 12a, we show a plot of magnetization vs time, for the amplitude of the axial field, $H_0 = 50D$, and angular frequency $\mathbf{w} = 10^{-2}$ radian- D/\hbar . We notice that the magnetization shows distinct plateaus and in each plateau, the magnetization oscillates a fixed number of times. The number of oscillation N_{osc} in each plateau is given by the ratio of half the energy gap between the $M_S = -10$ and the $M_S = -9$ states at the field H_0 and $\hbar\mathbf{w}$ where \mathbf{w} corresponds to the angular frequency of the applied axial field. This kind of oscillation with similar dependence of N_{osc} has been theoretically observed in the two-level systems by Rotvig *et al*³⁶ and Raghavan *et al*³⁷. Such oscillations have also been seen in the Bose–Einstein condensates in a double-well trap³⁸. Rotvig *et al*³⁶ observe this in the context of a two-band semiconductor superlattice in an external electric field, while Raghavan *et al*³⁷ observe it in a single-band model in the presence of an electric field. In these calculations, the probability in a given state shows the temporal oscillations that we see here for magnetization. Indeed, the different M_S states in the magnetic cluster can be viewed as forming a large but finite lattice. The transverse magnetic field couples the states at successive lattice sites, much as the transfer terms in the models of Rotvig *et al*³⁶

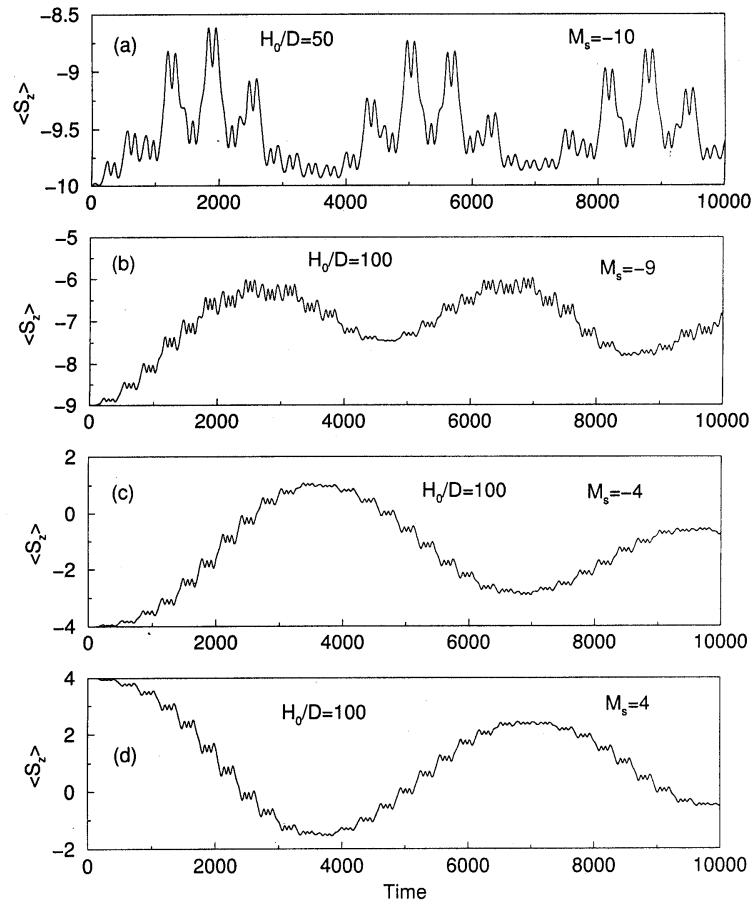


Figure 12. (a) Plot of evolution of magnetization with time (in units of $\hbar/D \times 10^{-1}$) for $H_0/D = 50$ and $\mathbf{w} = 0.01$ radian- D/\hbar , initial state is $M_s = -10$. For (b), (c) and (d) $H_0/D = 100$ and $\mathbf{w} = 0.01$ radian- D/\hbar , initial states are respectively $M_s = -9, -4$ and 4 .

and Raghavan *et al*³⁷. The time varying axial magnetic field corresponds to the applied oscillatory electric field of the two level systems. It is also worth noting that for the parameters that Raghavan *et al*³⁷ use, the oscillations die down for larger lattices. It appears that the size of the pseudo-lattice provided by the magnetic cluster is not large enough for the oscillations to die down for the realistic model parameters we have chosen.

The oscillations in magnetic field that we observe are quite robust. We have observed these oscillations for other initial states with integral M_S values corresponding to the eigenstates of the H_{dip} , with off-diagonal elements set to zero (figures 12b–d). The dependence of the magnetization on the amplitude of the magnetic field is shown in figure 13. We note that at higher fields, we see more oscillations in each plateau since the gap between successive M_S states widen with increasing amplitude. In figures 14b, d and f, we show the energies of the two low-lying eigenstates of H_{dip} , corresponding to the axial field at that instance. We note that the jump in magnetization coincides with two

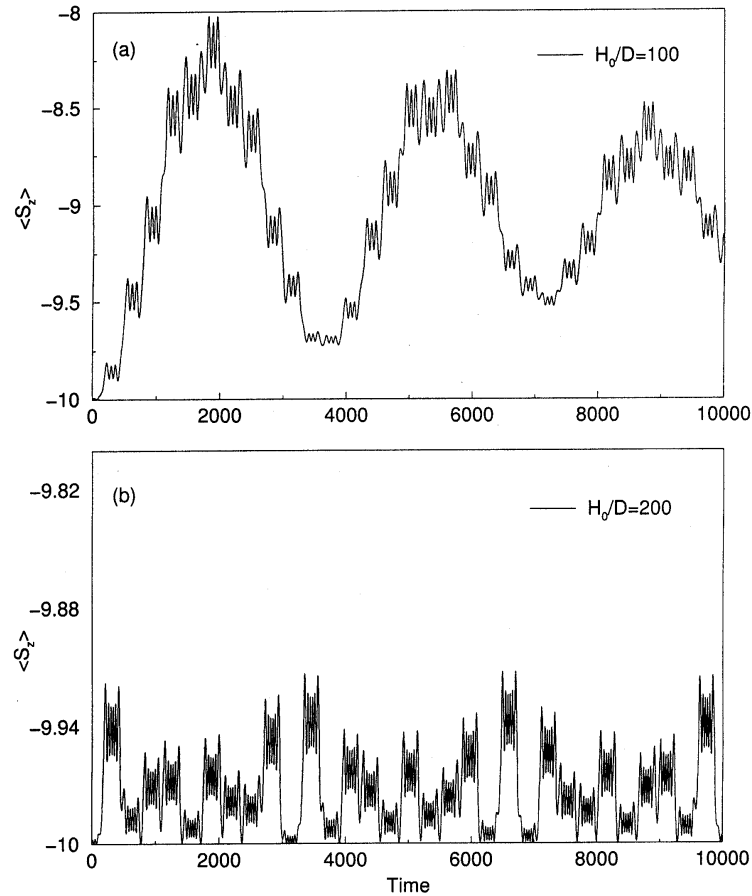


Figure 13. (a) Plot of magnetization vs time when $H_0/D = 100$ and $w=0.01$. For (b) $H_0/D = 200$ and $w = 0.01$. Initial state in both cases is $M_S = -10$. w and time are in units of figure 12.

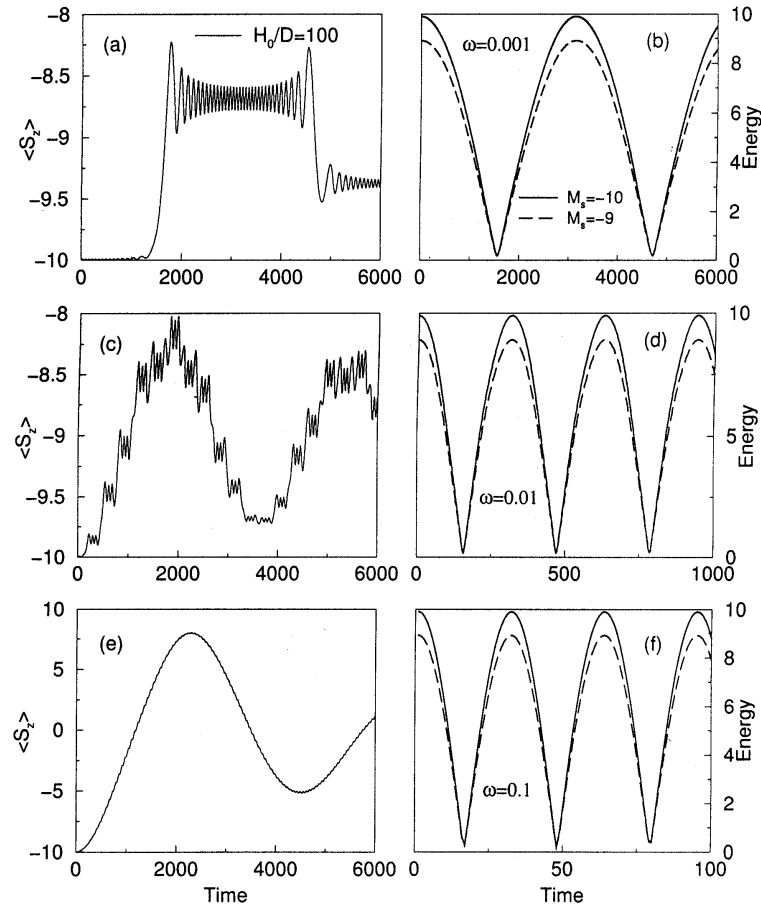


Figure 14. Magnetization vs time (a, c and e) and energy of $M_s = -10$ (solid line) and -9 (broken line) vs time (b, d and f) for (i) $\omega = 0.001$ (a, b) (ii) $\omega = 0.01$ (c, d) and (iii) $\omega = 0.1$ (e, f). $H_0/D = 100$ for all cases. ω and time are in units of figure 12.

states with different M_s values becoming degenerate. In the time between these coincidences, the magnetization shows small amplitude oscillations. Assuming that the system wavefunction evolves as $\exp(-i(\bar{E}_2 - \bar{E}_1)t/\hbar)$, where \bar{E}_1 and \bar{E}_2 are the average energies of the two states in question, the number of oscillation in a time period $t = 2\pi/\omega$ is given by $(\bar{E}_2 - \bar{E}_1) = \hbar\omega$. We note that the energy gap at the maximum amplitude in all the cases are the same and hence the number of oscillations in a plateau is inversely proportional to the frequency of the axial field. In figures 14a, c and e we show the dependence of the oscillation pattern on the frequency of the axial field with a fixed amplitude. We note that at decreasing frequencies, the number of oscillations in each plateau increases and the plateau structure itself vanishes with the magnetization following the magnetic field for higher frequency of the axial field.

We have also studied this system in the presence of an axial magnetic field with two different frequencies, given by $H_0 \cos(\mathbf{w}_1 t) \cos(\mathbf{w}_2 t)$. This leads to a beat pattern involving the sum and difference of the two frequencies. In figure 15, we show the time variation of

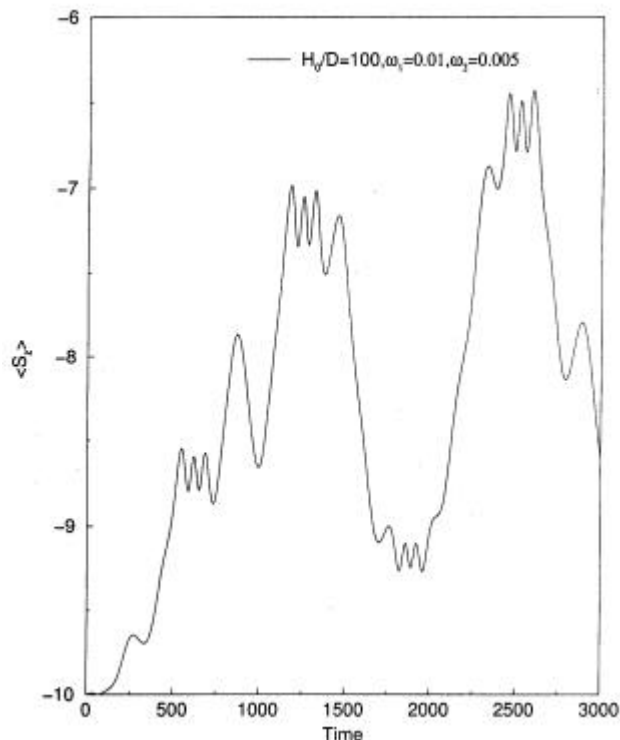


Figure 15. Plot of magnetization vs time when $H_0/D = 100$, $\omega_1 = 0.01$ and $\omega_2 = 0.005$. ω and time are in units of figure 12.

magnetization in the presence of two different frequency magnetic fields. We note that one set of oscillations correspond to $N_{osc} = \Delta E/2\hbar (\omega_1 + \omega_2)$ while another set of oscillations have $N_{osc} = \Delta E/2\hbar (\omega_1 - \omega_2)$, where ΔE is the difference in energy between the $M_S = -10$ and $M_S = -9$ states when the axial field is equal to the amplitude.

The parameters for which we have carried out the calculations corresponds to Mn_{12} . However, systems such as Fe_8 also have high spin ground state although the D value is different. In order to study the effect of change in D value on the oscillations, we have carried out these calculations for several H_0/D values. In figure 16, we show the results of our calculations for $H_0/D = 20$ and $H_0/D = 10$. The oscillations vanish ($H_0/D = 20$) and we have a M vs t behaviour that does not have much structure for this larger H_0/D value. However for lower H_0/D value, we find that the oscillations persist, but with much reduced amplitude. Thus, it is possible that in other high spin systems, these oscillations are found at different field amplitude.

7. Summary and conclusion

The synthesis of high nuclearity high spin magnetic clusters has provided an impetus for studying magnetism on a nanoscale. These systems are the magnetic analogs of quantum dots or artificial atoms fabricated using semiconductor structures. The magnetic clusters

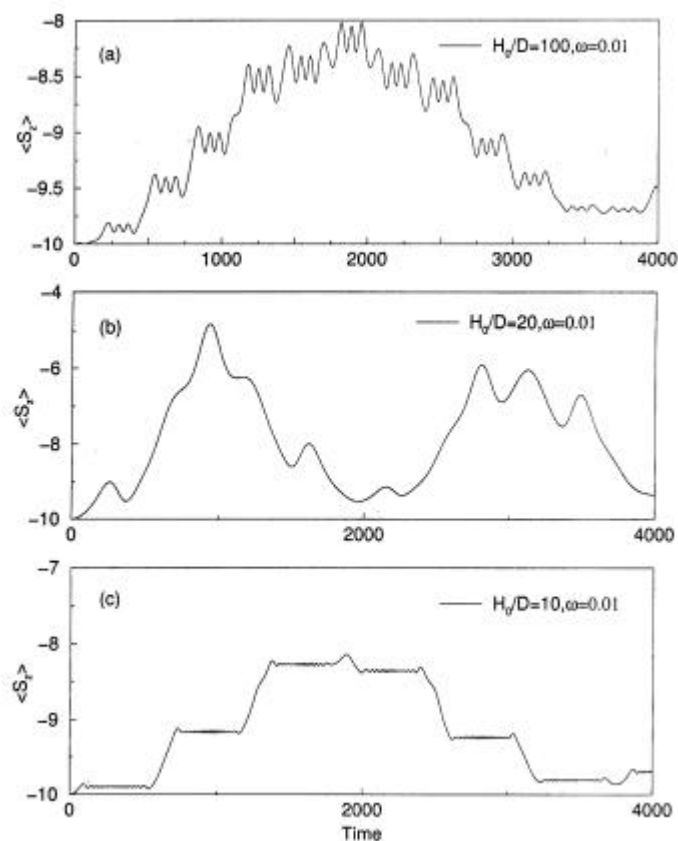


Figure 16. Evolution of magnetization with time with different H_0/D values, ω is kept fixed at 0.01. $H_0/D = 100, 20$ and 10 respectively for (a), (b) and (c). ω and time are in units of figure 12.

exhibit a wide variety of basic phenomena in a dramatic fashion. The quantum resonant tunnelling in these systems manifests as magnetization plateaus in a magnetization vs magnetic field plots. They also exhibit dynamic oscillations characterized by temporal localization in an oscillating magnetic field, much as the behaviour displayed by two level systems in an oscillating electric field.

Understanding these phenomena at a quantitative level requires devising methods for solving low-lying eigenstates of large exchange Hamiltonians as well as methods for studying time evolution of properties in these states, in the presence of off-diagonal perturbations. We have shown that simple time dependent techniques allow tracking the dynamics in these systems. Our studies, besides reproducing experimental observations quantitatively also predicts new phenomena such as dynamic oscillations in magnetization in high spin clusters.

Acknowledgement

This work has been partly supported by the Council of Scientific & Industrial Research, New Delhi through its extramural research grants awarded to SR and DS.

References

1. Lis T 1980 *Acta Crystallogr.* **B36** 2042; Delfas C, Gatteschi D Pardi L, Sessoli R, Wieghardt K and Hanke D 1993 *Inorg. Chem.* **32** 3099; Barra A L, Gatteschi D, Pardi L, Müller A and Döring J 1992 *J. Am. Chem. Soc.* **114** 8509
2. Gunther L and Barbara B (eds) 1995 *Quantum tunnelling of magnetization – QTM'94* NATO ASI Ser. E2 (Dordrecht: Kluwer) vol. 301; Friedman J R, Sarachik M P, Tejada J and Ziolo R 1996 *Phys. Rev. Lett.* **76** 3830; Thomas L, Lioni F, Ballou R, Gatteschi D, Sessoli R and Barbara B 1996 *Nature (London)* **383** 145, and references therein; Wernsdorfer W and Sessoli R 1999 *Science* **284** 133
3. Wernsdorfer W and Sessoli R 1999 *Science* **284** 133; Garg A 1993 *Europhys. Lett.* **22** 205, and references therein
4. Hotzelmann R, Wieghardt K, Flörke U, Haupt H, Weatherburn D C, Bonvoisin J, Blondin G and Girerd J 1992 *J. Am. Chem. Soc.* **114** 1681
5. Chiorescu I, Wernsdorfer W, Müller A, Bögge H and Barbara B 2000 *Phys. Rev. Lett.* **84** 3458
6. Roberta Sessoli *et al* 1993 *J. Am. Chem. Soc.* **115** 1804
7. Delfs C D, Gatteschi D, Pardi L, Sessoli R, Weighardt K and Hanke D 1993 *Inorg. Chem.* **32** 3099
8. Tupitsyn I and Barbara B 2001 Quantum tunneling of magnetization in molecular complexes with large spins. Effect of the environment. In *Magnetism – molecules to materials* JS Miller and M Drillon (New York: Wiley-VCH) (in press)
9. Chudnovsky E M 1996 *Science* **274** 938; Stamp P C E 1996 *Nature (London)* **383** 125; Thomas L, Lioni F, Ballou R, Gatteschi D, Sessoli R and Barbara B 1996 *Nature (London)* **383** 145
10. Perenboom J A A J, Brooks J S, Hill S, Hathaway T and Dalal N S 1998 *Phys. Rev.* **B58** 330; del Barco E, Hernandez J M, Sales M, Tejada J, Rakoto H, Broto J M and Chudnovsky E M 1999 *Phys. Rev.* **B60** 11898
11. Zener C 1932 *Proc. R. Soc. London* **A137** 696; Gefen Y, Ben Jacob E and Caldeira A O 1987 *Phys. Rev.* **B36** 2770; Ao P and Rammer J 1989 *Phys. Rev. Lett.* **62** 3004; 1991 *Phys. Rev.* **B43** 5397; Shimshoni E and Stern A 1993 *Phys. Rev.* **B47** 9523; Leuenberger M N and Loss D 2000 *Phys. Rev.* **B61** 12200
12. Katsnelson M I, Dobrovitski V V and Harmon B N 1999 *Phys. Rev.* **B59** 6919
13. De Raedt H, Miyashita S, Saito K, Garcia-Pablos D and Garcia N 1997 *Phys. Rev.* **B56** 11761; Garcia-Pablos D, Garcia N and De Raedt H 1998 *Europhys. Lett.* **42** 473
14. Barra A L, Gatteschi D and Sessoli R 1997 *Phys. Rev.* **B56** 8192
15. For a review see, Soos Z G and Ramasesha S 1990 *Valence bond theory and chemical structure* (eds) D J Klein and N Trinajstic (Amsterdam: Elsevier) p 81
16. Ramasesha S and Soos Z G 1993 *J. Chem. Phys.* **98** 4015
17. Raghu C, Rudra I, Sen D and Ramasesha S 2001 *Phys. Rev. B* (in press)
18. Hendrickson D N, Christou G, Schmitt E A, Libby B, Baskin J S, Wang S, Tsai H L, Vincent J B, Boyd W P D, Haffman J C, Folting K, Li Q and Streib W E 1992 *J. Am. Chem. Soc.* **114** 2455, and references therein
19. Chudnovsky E M 1996 *Science* **274** 938
20. Hennion M, Pardi L, Mirebeau I, Surad E, Sessoli R and Caneschi A 1997 *Phys. Rev.* **B56** 8819; Mukhin A A, Travkin V D, Zvezdin A K, Lebedev S P, Caneschi A and Gatteschi D 1998 *Europhys. Lett.* **44** 778
21. Reynolds P A, Gilbert E P and Figgis B N 1996 *Inorg. Chem.* **35** 545
22. Gorun S M and Lippard S J 1988 *Inorg. Chem.* **27** 149; Armstrong W H, Roth M E, Lippard S J 1987 *J. Am. Chem. Soc.* **109** 6318
23. Pontillon Y *et al* 1999 *J. Am. Chem. Soc.* **121** 5342
24. Rudra I, Sen D and Ramasesha S 2001 *Phys. Rev.* **B64** 14408
25. Friedman J R, Sarachik M P, Tejada J and Ziolo R 1996 *Phys. Rev. Lett.* **76** 3830
26. Hernandez J M, Zhang X X, Luis F, Tejada J, Friedman J R, Sarachik M P and Ziolo R 1997 *Phys. Rev.* **B55** 5858
27. Davidson E R 1975 *J. Comput. Phys.* **17** 87
28. Rudra I, Ramasesha S and Sen D 2001 *J. Phys. Condens. Mater.* (in press)

29. Leuenberger M N and Loss D 1999 *Europhys. Lett.* **46** 692; cond-mat/9907154; Callen E and Callen H B 1965 *Phys. Rev.* **139** A455
30. De Raedt H, Miyashita S, Saito K, Garcia-Pablos D and Garcia N 1997 *Phys. Rev.* **B56** 11761; Garanin D A and Chudnovsky E M 1997 *Phys. Rev.* **B56** 11102i; Garg A 1998 *Phys. Rev. Lett.* **81** 1513; Tupitsyn I S cond-mat/9712302; Prokofev N V and Stamp P CE 1996 *J. Low. Temp. Phys.* **104** 143; Katsnelson M I, Dobrovitski V V and Harmon B N cond-mat/9807176
31. Wannier G H 1960 *Phys. Rev.* **117** 432; 1962 *Rev. Mod. Phys.* **34** 645; Avron J E 1982 *Ann. Phys. (NY)* **143** 33; Fukuyama H, Bari R A and Fogedby H C 1973 *Phys. Rev.* **B8** 5579; Barticevic Z, Pacheco M and Claro F 1995 *Phys. Rev.* **B51** 14414; Gibb K, Dignam M M, Sipe J E and Roth A P 1993 *Phys. Rev.* **B48** 8156
32. Bloch F 1928 *Z. Phys.* **52** 555; Forst M, Segsneider G, Dekorsy T and Kurz H 2000 *Phys. Rev.* **B61** R10563; Kyriakidis J and Loss D 1998 *Phys. Rev.* **B58** 5568; Morifuji M and Hamaguchi C 1998 *Phys. Rev.* **B58** 12842
33. Agarwal G S and Harshawardhan W 1994 *Phys. Rev.* **A50** R4465, and references therein
34. Dunlap D H and Kenkre V M 1986 *Phys. Rev.* **B34** 3625; 1988 *Phys. Lett.* **A127** 438; 1988 *Phys. Rev.* **B37** 6622
35. Rudra I and Ramasesha S cond-mat/0105616
36. Rotvig J, Antti-Pekka Jauho and Smith H 1995 *Phys. Rev. Lett.* **74** 1831
37. Raghavan S, Kenkre V M, Dunlap D H, Bishop A R and Salkola M I 1996 *Phys. Rev.* **A54** R1781
38. Smerzi A, Fantoni S, Giovanazzi S and Shenoy S R 1997 *Phys. Rev. Lett.* **79** 4950